INL/JOU-21-63558-Revision-0

Water Interplays during Dysprosium Electrodeposition in Pyrrolidinium Ionic Liquid: Deconvoluting the Pros and Cons for Rare Earth Metallization

Abderrahman Atifi, Kennalee Orme, Donna L Baek, Robert V Fox

Changing the World's Energy Future

Idaho National Laboratory

INL is a U.S. Department of Energy National Laboratory operated by Battelle Energy Alliance, LLC

INL/JOU-21-63558-Revision-0

Water Interplays during Dysprosium Electrodeposition in Pyrrolidinium Ionic Liquid: Deconvoluting the Pros and Cons for Rare Earth Metallization

Abderrahman Atifi, Kennalee Orme, Donna L Baek, Robert V Fox

October 2021

Idaho National Laboratory
Idaho Falls, Idaho 83415

http://www.inl.gov

Prepared for the
U.S. Department of Energy
Under DOE Idaho Operations Office
Contract DE-AC07-05ID14517

Water Interplays During Dysprosium Electrodeposition in Pyrrolidinium Ionic Liquid: Deconvoluting the Pros and Cons for Rare Earth Metallization

[a] Kennalee Orme, [a] Donna L. Baek, [a] Robert V. Fox, [a] Abderrahman Atifi*

[a] *Critical Materials Institute, Chemical Systems Department, Idaho National Laboratory, Idaho Falls, Idaho 83415, United States.*

Corresponding Author

* A. Atifi *abderrahman.atifi@inl.gov*

KEYWORDS: Dysprosium, Electrodeposition, Ionic Liquid, Water, Speciation Heterogeneity, Reduction Mechanism, Interfacial Processes, Metal Stability and Purity.

ABSTRACT: The electrochemical production of rare earth metals (REMs) in ionic liquids (ILs) has received much attention as a promising, sustainable replacement to molten salt electrolysis. Water additives have been suggested as a promoting strategy for the ionic liquid process, however the fundamental understanding of the interfacial processes

required to assess the overall viability for REM production is lacking. In this regard, a full investigation of water impact on dysprosium (Dy) electrodeposition in pyrrolidinium triflate (BMPyOTf) ionic liquid was carried out. Water introduction was revealed to involve an interplay of implications on the electrodeposition process, including coordination, speciation, reduction pathways, interfacial dynamics, nucleation and metal stability and purity. In highly dry conditions, the reduction occurs at very negative potentials (-3.3V) in a consecutive pathway, resulting in negligible metal electrodeposition (low rate and efficiency) at the electrode surface. Small water concentrations (<500ppm) lead to partitioning of the Dy complex between water and IL coordinated speciation, giving rise to an additional wave at more positive potentials (-2.4V). Probing the heterogeneous Dy speciation by spectroscopic analyses enabled uncovering of the reduction mechanism and evaluation of the mass transport properties. In addition to lowering the reduction thermodynamics, water introduction also improved the nucleation, deposition rate and faradaic efficiency. Despite these benefits, stripping voltammetric analysis predicts substantial chemical reactivity of the deposited Dy metal with water additives and/or electrolyte components, under long timescales. Surface characterization of the obtained product confirmed Dy metal instability as oxidized/fluorinated material and limited purity (~60%). Moreover, high water introduction triggered a fast hydrogen evolution reaction (HER), downgrading the robustness of system efficiency. The overall impact of water additives seems to

engender both promoting and mitigating effects on electrochemical REM production in IL, requiring a specific technoeconomic assessment and/or more innovative strategies to be sought.

INTRODUCTION: Continued electrification of society has driven demand for metallic forms of rare earth elements (REEs) used in microelectronics, electricity generation (e.g., windmills and hydroelectric turbines), and in transfer of stored electricity (electric vehicle traction motors ([1,2]). Rare earth permanent magnets found in electricity generation turbines and electric vehicle motors are comprised primarily of iron, with up to 30% (wt.%) neodymium, and smaller concentrations of dysprosium and terbium (~1.4–11.0 wt.%), which impart resistance to demagnetization at higher operating temperatures (3). As a consequence of a high and immediate market demand, a secure supply chain of the rare earth metals (REMs) has become a critical component for the sustainability of today's economy ([1,3,4]). Currently, the industrial production of REMs occurs either by thermal reduction of fluoride salts using calcium, which is a batch process requiring several downstream purification steps, or by molten fluoride salt electrolysis, which is amenable to continuous-production methodology and has become the predominant industrial technique that is primarily practiced in Asia ([5]). REM production through molten salt electrolytes involves the use of lithium fluoride, due to the high solubility of

rare earth oxides. The primary drawbacks to currently practiced molten salt electrolysis are the production of gaseous pollutants (CO, CO_2, HF, perfluorocarbons), production of toxic fluoride salt wastes, and the thermal energy requirement to maintain high bath temperatures (~1000 °C) ([2,6]).

Alternative, low-temperature and environmentally friendly electrochemical reduction methods have been investigated recently for the production of metallic-state transition metals, alloys, and rare earth elements in ionic liquid electrolyte systems ([7–9]). Owing to their unique properties including intrinsic conductivity, large electrochemical window and low vapor pressure, REE electrodeposition in ionic liquids would offer lower energetic and environmental bills ([10–14]). However, electroreduction of REE at low temperatures in these media faces several key challenges. From technical point of view, the electrolyte must offer high diffusivity and metal loading capacity, with a wide electrochemical window (EW). The most prominent and noteworthy work has been accomplished by Matsumiya et al. at the Yokohama National University (Japan) ([15–21]) . In that body of work the most significant technical challenges consisted of limited product stability, purity and deposition rate, compared to the molten salts process. After more than a decade of attempts, only marginal success has been made, with no reporting to date of an economically feasible pilot-scale system.

As one of the highly targeted REMs, research on Dy electrodeposition in several ionic liquid-based electrolytes has been active in the last decade ([16,22–28]). Dysprosium's high intrinsic coercivity enables NdFeB magnets to maintain performance at high temperatures ([29]). Early work on Dy reduction was reported by Lodermeyer et al., where efficient deposition could be achieved in a mixture of organic solvent and ionic liquid ([22]). Matsumiya and co-workers have extensively studied Dy electrodeposition in phosphonium ionic liquids, where the reduction occurs at very negative potentials (-3.5V vs Fc^+/Fc) and proceeds through both consecutive (1+2e-) and one step (3e-) mechanisms ([16,23–26]). In pyrrolidinium ionic liquids, the reduction followed a single step reduction, with much more positive potentials than in phosphonium class ([27,28]). While these efforts have established the proof of concept of the ionic liquid process, achieved deposition rates were still sluggish compared to the molten salt process. The major drawbacks of using ionic liquids were due to high viscosity and low metal loadings, which lead to limited mass transport.

Several strategies have been proposed to overcome the ionic liquid limitations, with the increase of operating temperature, use of organic solvents and neutral ligand-based ionic liquids having been explored ([15,30–35]). Of interest to this work, water has been reported as a good promoter for the electrochemical REMs production in ionic liquids ([33,34]). Early work on water impact was reported by Matsumiya et al., where slight

increase of water content (100 to 200ppm) in phosphonium ionic liquids switched the reduction process from a consecutive (1+2e-) reductions into a one-step (3e-) pathway ([16]). In addition to this switch, the peak current decreased and the reduction potential shifted to more negative values. Those changes were ascribed to formation of an aqua complex that requires larger overpotential for reduction. Recent reports on Nd reduction in similar ionic liquids demonstrated that water additives exhibited quite opposite changes ([33]). As result of positive shift and current increase, introduction of water led to the increase of Nd recovery by three times and dense layers of the electrodeposited metal were collected. In more extended study, the authors reported the formation of a Nd complex with mixed coordination sphere, containing both water and bistriflimide anions ([36]). Similarly, promoting effects of water addition were reported in Eu electrodeposition in dicyanamide ionic liquid ([34]). In that work, the reduction also shifted to more positive potentials, following a consecutive 1+2e- process. However, surface analysis of the obtained electrodeposit materials reveals an oxidized form of Eu, due to simultaneous chemical reaction with added or residual water.

Given the complex coordination and interfacial interplays, water additives are expected to result in severe alterations of the reduction process in ionic liquids. In reviewing the reported works on water introduction, it becomes evident that the electrochemical behavior should be highly dependent on the nature of the formed speciation. Yet,

examination of the correlation between the observed voltammetric response and evolving speciation heterogeneity in the presence of water is lacking. Although several complexes bearing different spheres and modes of coordination could be formed upon water introduction, the interpretation of reduction pathways (consecutive vs single step) has been mostly speculative. At the same extent, and given the deposition nature of the reduction process, not much attention has been dedicated to the stripping features during voltammetric analysis. As such, emergence of a surface (sharp) oxidative peak in the backward potential scan should be key indication about the stability of the REM under voltammetric timescale. Moreover, the evidence of metal stability and purity in water-rich ionic liquids is still lacking, mainly due to ambiguous product characterization, which raises the question about the promoting effects of water additives to produce REMs.

In previous work we undertook an investigation exploring the electroreduction of dysprosium triflate $Dy(OTf)_3$ complex in pyrrolidinium triflate (BMPyOTf) ionic liquid ([37]). The electrodeposition of $Dy(OTf)_3$ in BMPyOTf was shown to exhibit two reduction waves. Voltammetric analysis suggested the presence of two co-existent speciation in solution, bearing different coordination environments. Probed and consolidated by spectroscopic analyses, the heterogeneous speciation consisted of weakly and strongly IL-coordinated complexes at higher metal loadings. As result of the speciation

heterogeneity, the reduction mechanism was proposed to be more consistent with 2x3e- process, as compared to the commonly reported consecutive (1+2e-) process for doubly featured voltammetry. In spite of this proposal, factors driving the speciation heterogeneity and its coordination nature remained unclear. In the present work, impact of water inclusion in the metal coordination sphere will be investigated, as one potential driving factor for the speciation heterogeneity in ionic liquid. Interpretation of the reduction mechanism and interfacial processes will be discussed as a function of the water-induced speciation heterogeneity. The results of the mechanistic analysis will be correlated to the observed electrodeposition metrics (rate and faradaic efficiency) and product properties (metal stability and purity). Our approach is based on combining a full set of analytical tools, including voltammetry, chronoamperometry, surface characterization, spectroscopy and computational analyses. The outcomes of this study shed light on the overall water implications on the electrodeposition process, while assessing the viability of such a strategy for low temperature electrochemical production of REMs in ionic liquids systems.

EXPERIMENTAL AND METHODS

Chemicals and Preparation:

Dysprosium triflate ($Dy(OTf)_3$, 99.5%) was purchased from Strem Chemicals. 1-Butyl-1-methylpyrrolidinium triflate (BMPyOTf, 99.5%) ionic liquid was purchased from IoLiTec. Anhydrous acetone (99.8%) used in the rinsing of electrodeposited materials was purchased from Acros Organics. Trace metal grade nitric acid (HNO_3, 67-70%) was purchased from Fisher Chemical and used in the dissolution of electrodeposited materials. Preparation of $Dy(OTf)_3$ in BMPyOTf solution was conducted in a glovebox under argon atmosphere (H_2O <10 ppm, O_2 <1 ppm). Specific H_2O concentrations in solutions of $Dy(OTf)_3$ in ionic liquid were achieved by dissolving either dried (under vacuum for over 5 h at 90 °C) or as received $Dy(OTf)_3$ in dried (under vacuum for over 8 h at 90 °C) BMPyOTf. Dry $Dy(OTf)_3$ produced solutions with low H_2O concentrations, while the non-dried $Dy(OTf)_3$ produced solutions with higher H_2O concentration. These solutions were combined to obtain solutions with H_2O concentrations ranging from 30 to 3500ppm, which were confirmed using Karl-Fisher (KF) analysis.

Electrochemical Measurements:

Electrochemical analysis was performed using a Bio-Logic SP-150 Potentiostat. Voltammetric experiments were carried out using a standard three-electrode configuration. Platinum discs (1.5 and 3.0mm diameter) were used as working electrodes, while platinum wires were used as pseudo-reference and counter electrodes. In the case of chronoamperometric electrodeposition experiments, 3.0mm platinum

disc or copper plates were used as the working electrode, where cathodic and anodic compartments were separated with the use of glass frit. Ferrocenium/ferrocene (Fc^+/Fc) couple was used as an internal reference system in order to correct for potential shift of the employed platinum pseudo-reference. Given the significant viscosity and solution resistance in ionic liquids, the voltammograms were recorded with iR drop compensation. All electrochemical experiments were conducted in a glovebox under argon atmosphere. The cleaning procedure for working electrodes involved first removing ionic liquid from the electrode surface using a Kimwipe; the electrodes were then placed in 10% HNO_3 solution (diluted from 70% HNO_3 using 18MΩ H_2O), where any deposited materials were allowed to dissolve completely. After dissolution, the electrodes were rinsed with 18MΩ H_2O, rinsed with acetone, and dried under argon flow before being transferred into the glovebox. Counter and pseudo-reference electrodes were cleaned by rinsing with acetone before drying under argon flow. The surface of the working electrode was preconditioned with voltammetric scans in a separate metal-free ionic liquid solution.

Bulk, Surface, and Headspace Analyses:

Near IR (NIR) spectra of solutions were taken in a quartz cuvette that had been dried under argon flow. FTIR spectra were acquired using an ATR apparatus with minimal exposure to air during spectra collection. Total-reflectance X-ray fluorescence

spectrometry (TXRF) analysis was performed with a Bruker S2 Picofox TXRF spectrometer, using a selenium standard and a scan time of 1000s. The deposits were rinsed with anhydrous acetone, then allowed to dry under argon atmosphere. After cleaning, the deposits were taken from the glove box and dissolved in 10% HNO_3. In the preparation of samples for energy-dispersive X-ray coupled to scanning electron microscopy (EDS-SEM) and X-ray photoelectron spectroscopy (XPS), Dy was electrodeposited on copper plates. It was then washed with anhydrous acetone, to remove ionic liquid traces, dried and sealed inside the glove box. For gas chromatography (GC) analysis, headspace of electrodeposition cell was sampled before, during, and after electrodeposition of Dy. In the before and during samples, a needle was used to draw air from the headspace within the electrochemical cell before it was injected into a separate vial sealed with a septum cap, after which the samples were taken for analysis. For the post sample, the cell was sealed within the glovebox using a septum and the air was sampled for analysis from the cell headspace directly. NIR spectra were collected on a Shimadzu UV 3600 Plus, using 0.5 nm resolutions. FTIR spectra were recorded on a Bruker Ram II Vertex 70, using $1cm^{-1}$ resolution and 64 scans. Total-reflectance X-ray fluorescence spectrometry (TXRF) analysis was performed with a Bruker S2 Picofox TXRF spectrometer, using a selenium standard and a scan time of 1000s. Morphological and elemental characterization of the Dy deposit was performed with energy-dispersive X-ray spectroscopy coupled to scanning electron

microscopy (EDS-SEM, JEOL JSM 6610LV). X-ray photoelectron spectroscopy (XPS) was conducted using a using a Kratos Axis Ultra DLD spectrometer. GC spectra were collected using a Shimadzu Nexis GC-2030 instrument with fused silica columns Varian PoraPLOT U (25m, 0.32mm ID, 10um film thickness) and Restek RT-Msieve 5A (30m, 0.32mm ID 30um film thickness).

Computational:

Spectral deconvolution of mid and near infrared were performed using GRAMS (Thermo Scientific) software. XPS peak position was internally referenced to the C1s peak at 284.6 eV and fitted with Avantage software. Convolution electrochemistry was performed using DigiElch (Elchsoft) software to generate semi-integral and semi-derivative voltammetric traces.

RESULTS AND DISCUSSION

1) *Voltammetry:*

Dy reduction in ionic liquids has been reported to follow both consecutive two steps (1+2e-) and single step (3e-) pathways ([16,23,27,28]). In the previous study, the voltammetry of $Dy(OTf)_3$ reduction in BMPyOTf was shown to exhibit two reduction waves and one main oxidation peak at about -2.3V, -2.8V and 0V, respectively ([37]). The forward features

were assigned to reduction processes, leading to deposition of Dy metal on the surface, while the sharp oxidation peak during the backward scan is due to oxidative stripping of the Dy metal from the surface. Evolution of the voltammetric response from one main reduction (Red2) peak at low metal concentration to two waves at higher concentrations suggested the reduction of two co-existent speciation in solution. The first positive (Red1) wave was assigned to a 3e- reduction of weakly IL-coordinated metal complex to form the Dy metal. This assignment was also supported by the observed reversible features of the Dy(II)/Dy(III) wave at more positive potentials (-1V vs Fc^+/Fc) and the oxidative stripping peak (at 0V vs Fc^+/Fc) when scanning the potentials at the first reduction wave.

While the heterogenous speciation in our system was previously supported, exact factors altering the coordination spheres of Dy complexes were still unclear ([37]). Residual water traces in the dried ionic liquid are quantified at about 30ppm, excluding the effect of ionic liquid impurities as promotor for the heterogeneous speciation. However, another source of water could potentially stem from the hygroscopic nature of the dysprosium triflate complex, before and after its dissolution in the dried ionic liquid. In this work, quantification of water content of ionic liquid solutions containing 100mM of Dy-triflate complex showed about 3500ppm. Given the highly dried ionic liquid (~30ppm) and inert argon environment during dissolution, the obtained large water

concentration indicated that an approximately 5% water impurity was contained in the as-received product. Elemental quantification of Dy in the commercial product with TXRF analysis shows about 24% (vs weight) of Dy, compared to expected 27% in pure product (Table S2). Hence, such water content (3-5%) could have potential impact on the speciation as well as the electrodeposition process. To study this impact in more details, the water content in metal-containing solutions was monitored within a range of two orders of magnitude. Voltammetric inspection of 100mM $Dy(OTf)_3$ in BMPyOTf at platinum electrode was initially performed in dry conditions, as displayed in Figure 1a. At very small water traces (35ppm), the voltammetry shows two reduction waves at about -1.3V and -3.35V, respectively. The first wave exhibits significant chemical reversibility during the backward scan, with a half potential about -1.3V. The positive potential and chemical reversibility of this wave are consistent with 1e- reduction to form Dy(II) intermediate ([37]). The second more negative wave, shouldering the cathodic decomposition of the pyrrolidinium ionic liquid, had no corresponding oxidation peak during the backward scan (to about +1.5V vs Fc^+/Fc). Additionally, the peak current appears to be much higher than 2e- transfer, relative to 1e- Dy(II) wave. This could be indicative of potential contribution of catalytic current (EC'), due to reactivity of Dy metal with electrolyte components.

Introduction of small water concentrations (200ppm) leads to substantial changes in the voltammetric response. Main variations were the emergence of new reduction wave at more positive potentials (-2.3V), with a corresponding oxidation peak at about +0.1V (Figure 1a). Additionally, significant decrease in current intensity of the more negative wave was observed. While the latter seems to be screened by the Cottrell decay of the emerging wave, Red2 wave could still be observed upon multiple potential scans (Figure S2). Evaluation of peak current (J_p) densities as a function of the square root of scan rate ($\nu^{1/2}$) shows a linear relationship, as expected for a diffusion-controlled reduction process (Figure S1). These observed features, including the positive potential, significant chemical reversibility and sharpness of the oxidation peak are all consistent with Red1 wave that is observed at higher water contents. Hence, the emerging wave (Red1) is assigned to 3e- reduction of Dy(III) to Dy (metal). In fact, water introduction seems to switch the reduction from consecutive (1+2e-) to a single step (3e-) pathway. Similar impact on the reduction mechanism has been observed in phosphonium-based ionic liquid ([16]). However, in that reported study, the peak current decreased and the reduction potential shifted to more negative values, when the water content changed from 100 to 200ppm. Under the present conditions, the water introduction exhibited quite opposite effects, mainly a positive potential shift and current increase. These observations are in agreement with reported effects of water introduction on Nd and Eu reduction in ionic liquids ([33,38]).

While REE reduction engenders metal deposition, factors controlling its oxidative stripping from the surface have not been well explored. The magnitude of stripping charge, relative to the reduction component, is proportional to the stable fraction of the deposited metal. For a chemically reversible metal electrodeposition, the stripping ratio is expected to be independent of scan rate ([39]). To assess the chemical stability of the electrodeposition process under our experimental conditions, CV traces were recorded at different scan rates (Figure 1c). At higher scan rates, the stripping charge ratio (Q_{Ox}/Q_{Red}) reached a value of 35%, while decaying to about 15% at lower scan rates. Additionally, scanning the potential at first or both reduction waves exhibited similar stripping ratios (~30%), indicating that both processes would hold comparable chemical reversibility.

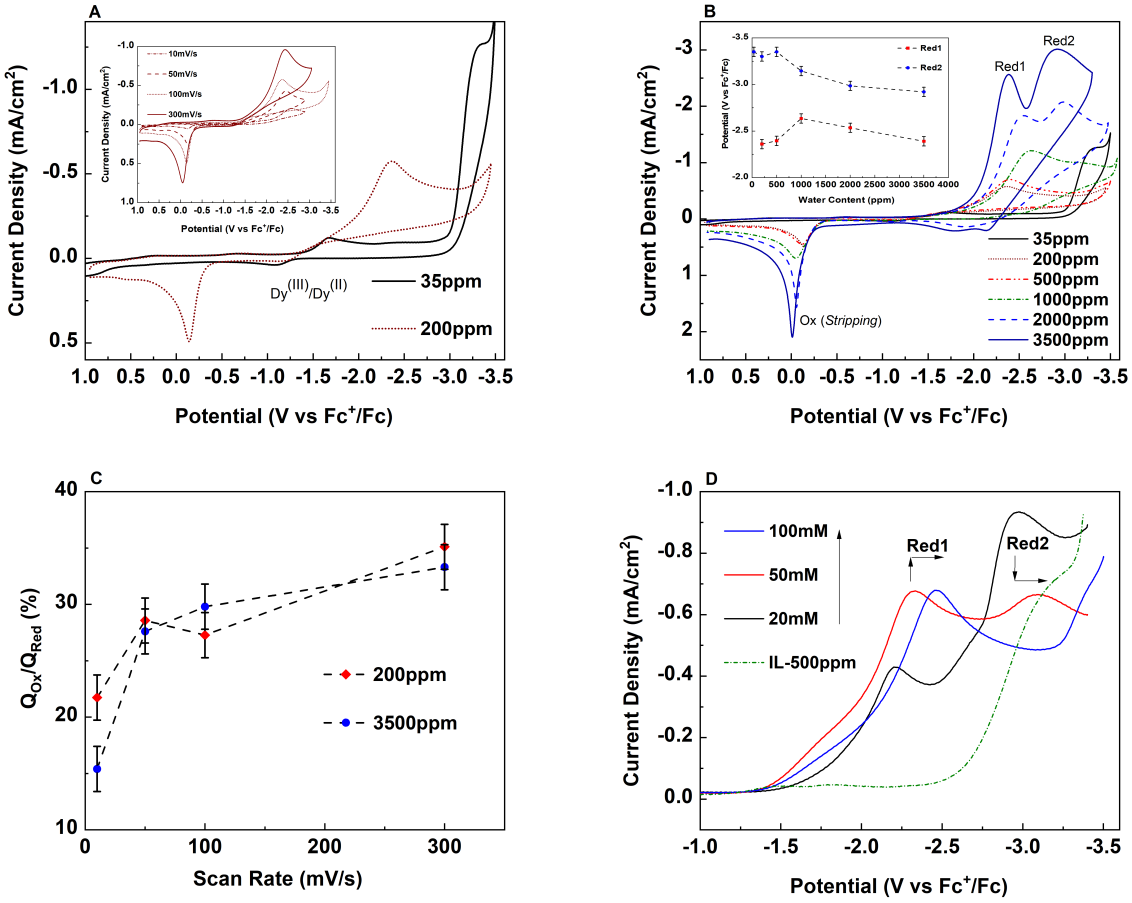

Figure 1. A) CV traces of 100mM $Dy(OTf)_3$ in BMPyOTf at two different water contents (35 and 200ppm). Inset: CV traces of 100mM $Dy(OTf)_3$ in BMPyOTf with 200ppm water content at different scan rates (mV/s). B) CV of 100mM $Dy(OTf)_3$ in BMPyOTf at different water contents (ppm). Inset: potential shifts of Red1 and Red2 as a function of water content (ppm). C) Stripping % at two different water contents (ppm) and different scan rates (mV/s). D) LSV traces of 20, 50 and 100mM $Dy(OTf)_3$ in BMPyOTf at $[H_2O]$=500ppm.

To further investigate the nature of the emerging wave (Red1) and the more negative wave (Red2), voltammetric traces were recorded at an extended interval of water contents (Figure 1b). Increasing the water content to 3500ppm resulted in continuous growth of Red1 and oxidation peak as well as shifting the peak potentials of both reduction waves. The potential shifts of both reduction waves as a function of water content are illustrated in Figure 1b (Inset). Small water additives (from 35 to 500ppm) mainly leads to emergence and growth of Red1, with no significant shifts in peak potentials. At water contents above 500ppm, both waves are gradually shifted to more positive potentials, with increased current intensities. As a result, difference in peak potentials (ΔE_{12}) between the two waves collapsed by about 0.5V (from 1 to 0.5V). The changes displayed by the voltammograms at intermediate water contents clearly demonstrate the evolution of the more negative wave (-3.3V) at 35ppm into previously assigned Red2 (-2.9V) at 3500ppm.

It is then evident that evolution of the voltammetry from one into two reduction waves is well correlated with water content in the system. Recent work on the reduction of neodymium bistriflimide complex in mixture of phosphonium ionic liquids, containing triflate and bistriflimide anions, exhibited two reduction waves ([40]). However, the reported processes were tentatively assigned to either a consecutive mechanism or different coordination environments. In fact, water coordination to the metal center

could promote different coordination spheres around the metal center. In very dry media, the metal complex is expected to be highly coordinated to ionic liquid anions. The coordination number of Dy(III) has been reported to be between 8 and 10, with 3 bidentate ligands and additional (mono/bidentate) ligation to ionic liquid anions, resulting in an overall charge of -2 ([25]). With such a highly negative charge, the IL-coordinated complex would encounter substantial electrostatic repulsion with the negatively charged electrode surface, leading to limited substrate disposition at the interface. Due to these electrostatic penalties, the reduction process of Dy complex is thermodynamically harder in dry ionic liquid media. Water introduction into the system would partially displace the ionic liquid anions, leading to two partitioned speciation in solution. Upon water coordination, the total negative charge of the Dy complex could be lowered (to -1 or 0), decreasing the electrostatic repulsion at the electrified interface. As a result, the reduction thermodynamics for the water-coordinated speciation becomes easier. At higher concentration, water seems to alter the more negative reduction wave, causing a significant potential shift to more positive values. In a water-rich environment, side reactions such as Dy metal oxidation and/or direct water electrolysis at the surface may be accelerated, triggering the hydrogen evolution reaction (HER). Overall, the impact of water coordination is shown to be correlated with the evolution of speciation heterogeneity. In agreement with our prior report, the water-coordinated speciation (Dy-H_2O) could be then envisioned as the previously assigned

weakly IL-coordinated speciation, which is reduced at positive potentials (Red1). Whereas, the IL-coordinated (Dy-IL) speciation, previously described as strongly IL-coordinated complex, is reduced at the more negative potentials (Red2).

To consolidate the correlation between water introduction and heterogeneous speciation, voltammetric inspection was carried out at different metal loadings, under constant water content. Figure 1,d displays the recorded voltammograms at 20, 50 and 100mM of $Dy(OTf)_3$ in BMPyOTf, as well as the metal-free ionic liquid, at 500ppm water concentration. At 20mM, Dy reduction features two waves at -2.1 and -2.8V, with much higher peak currents for the Red2 (I_{p2}), as compared to Red1 (I_{p1}). Background voltammogram in metal-free solution (dashed line) shows the water reduction at much more negative potentials than Red1 wave, but comparable to Red2 wave. Increasing the metal concentration (from 20 to 50 and 100mM) leads to substantial rise in Red1 current, with significant shift of Red2 wave to more negative potentials. These observations are consistent with Dy partitioning between water-coordinated and IL-coordinated speciation. Similar impact of ionic liquids solvation and coordination on the redox behavior of organic and inorganic systems and their implications in many electrochemical processes have been extensively reported by Atifi et al. ([41–48]). At equimolar fraction, the water molecules would be partially coordinated to the Dy complex (Red1), with important fraction remaining as free or weakly-coordinated

molecules. Increasing the metal loading (or lowering x_{H2O}) increased the fraction of metal-coordinated water (Dy-H_2O) at the expense of free or weakly-coordinated water (IL-coordinated complex), resulting in a rise of Red1 at the expense of Red2. The current decrease and negative potential shift in Red2 are suggestive of high coupling between the reduction of the IL-coordinated Dy complex and water electrolysis.

2) Spectroscopy:

Previously we reported NIR characteristics of the heterogenous speciation at 1930 and 1970nm, which were assigned to different coordination spheres of Dy complexes ([37]). In that report, absorbance of the weakly IL-coordinated complex was shown to increase with the metal loading. While most reported electronic transitions are observed at 700, 900, 1200 and 1600nm, these low energy transitions were tentatively assigned to overtones and combinations bands ([16,23]). To further examine the correlation of water content with the speciation heterogeneity, NIR spectrum was monitored at different water concentrations. As surveyed in Figure 2a, no NIR absorbance (in the range 1850-2000nm) were observed in the highly dried (<35ppm) solution, indicating that both previously observed peaks (1930 and 1970nm) are related to water presence. Thus, the fully IL-coordinated metal complex, under very dry conditions, exhibits a blank absorbance in the studied NIR region (1850-2000nm). Notably, initial water introduction

(<500ppm) leads to emergence of one main NIR peak around 1970nm. At higher water concentrations (>500ppm), an additional shouldering peak at 1930nm is observed. Control experiments with added water to metal-free solutions shows a one main peak at 1930nm (dashed line in Figure 2a). In fact, the observed NIR features are consistent with free or weakly coordinated (1930nm) and strongly coordinated (1970nm) water to the Dy metal center. This assignment is also supported by spectral changes upon increasing metal loading at constant water concentration. As such, maintaining the water content at 1000ppm and increasing the metal complex concentration from 20 to 100mM, led to increased absorbance of 1970nm at the expense of 1930nm peak (Figure 2b). These changes demonstrate an increase of water coordination (vs free water) to the metal center upon introducing higher amount of metal complex. The observed variations are consistent with previously observed features in highly metal-loaded solutions ([37]).

The NIR results corroborate the voltammetric interpretation and provide more accurate assignment of electronic transitions upon increasing the metal loadings. Given the blank absorbance of the IL-coordinated speciation, the 1970nm peak is characteristic of the water-coordinated complex that is formed upon displacement of IL anion. Such water-coordinated (or weakly IL-coordinated) speciation emerges at low water concentrations or at high (saturated) metal loadings. In addition to these two (Dy-H_2O and Dy-IL) co-existent Dy complexes, it is unclear whether the 1930nm feature is strictly characteristic

for the free water or due to a third mix-coordinated complex, where water could be weakly (second sphere) coordinated the metal center. This latter peak is dominant at low metal loading and/or in water rich environment.

To investigate the correlation of water introduction with changes in coordination spheres, the IR spectrum of metal-containing solutions was monitored at different metal loading and water content. Figure 2c,d shows the two major changes observed in the finger-print region of the IR spectrum. The 1334 and 1054cm^{-1} are assigned to the asymmetric stretching of SO_3 and SO_3/CF_3 modes in the coordinated triflate anions, respectively ([49]). Increasing water content resulted in shifts towards lower energies, from 1334 and 1054cm^{-1} to 1323 and 1048cm^{-1}, respectively. Based on previous DFT calculations, a shift to lower energies was indicative of weak coordination of triflate anion (OTf^-) to the Dy metal center([37]). The triflate coordination to the metal center was shown to exhibit a 75cm^{-1} upshift, from 1250 to 1330cm^{-1}, between the free and coordinated anion. The observed shift of OTf^- stretching to lower energies was then consistent with weaker IL coordination at higher metal loading.

Addition of water diminishes the characteristic peaks of coordinated triflate (1334 and 1054cm^{-1}), resulting in broad bands that shift to lower energies (1322 and 1048 cm^{-1}). As control experiments, recorded spectra with added water (at same ppm) to metal-free solution did not show any of these observed vibrational changes. This is consistent with

displacement of ionic liquid OTf^- ligands by water molecules and emergence of water-coordinated species. Closer examination of these changes in highly water rich conditions shows the loss of isosbestic points in these intermediate spectra, indicating the presence of more than two speciation. This could suggest the formation of third complex with a mix-coordinated species between water and IL ligands or species bearing a different coordination number and type (mono vs bidentate) at higher water content. In such case, the water coordination to Dy metal center is expected to be weak, as indicated by NIR feature at 1930nm.

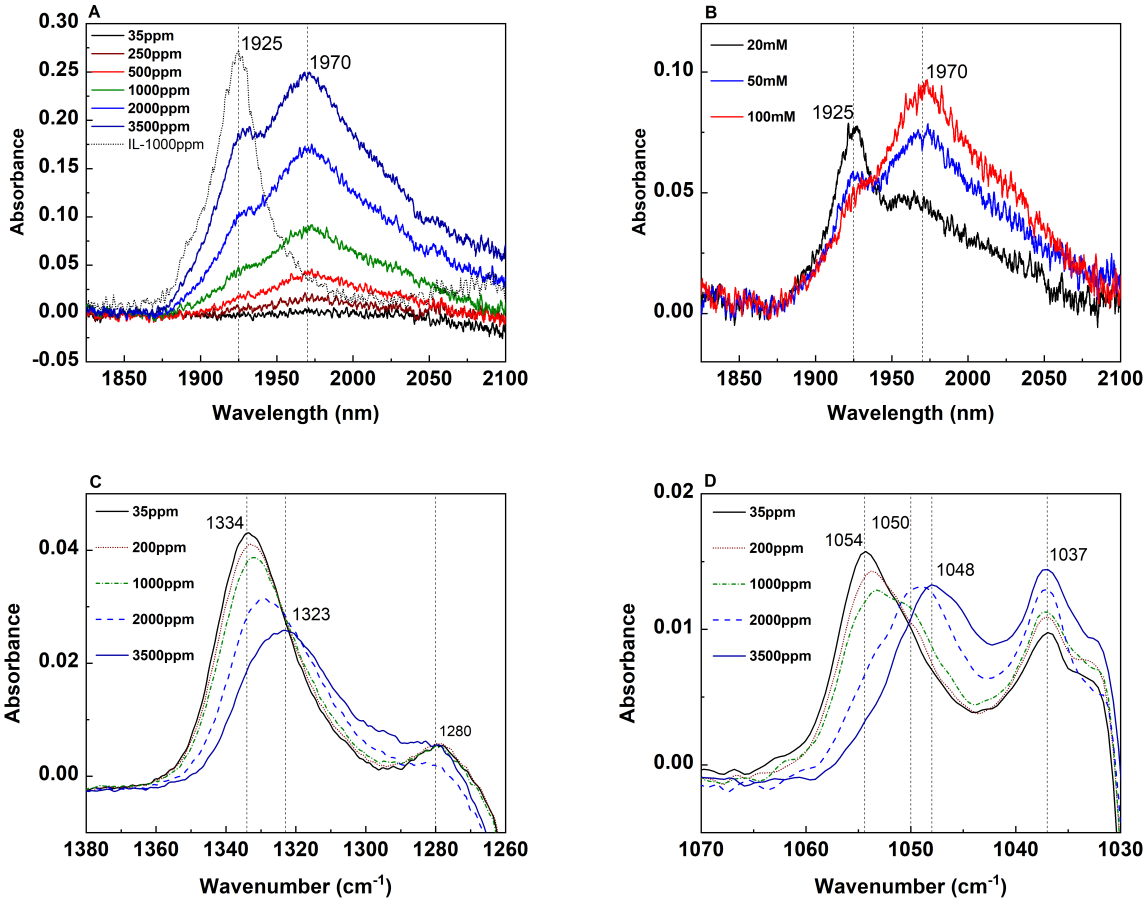

Figure 2. A) Recorded NIR spectra of 100mM $Dy(OTf)_3$ in BMPyOTf at different water contents (ppm). B) Recorded NIR spectra of 20, 50 and 100mM $Dy(OTf)_3$ in BMPyOTf at $[H_2O]$=1000ppm. C) and D) Recorded IR spectra of 100mM $Dy(OTf)_3$ in BMPyOTf at different water contents (ppm).

Similar to CV and NIR analyses, Figure S4 (solid lines) displays the observed changes of the IR spectrum in different metal loadings at constant water content (500ppm). At lower metal loading, the peaks 1334 and 1054cm^{-1} look pretty broad and could be deconvoluted to two vibrational bands, corresponding to water and IL-coordinated species. Spectral deconvolution of the broad IR bands reveals the individual peaks of the co-existent speciation and their computed molar fractions (Figure 3a,c). Consistent with voltammetric and NIR analyses, raising the metal concentration led to higher partitioning into the IL-coordinated speciation (vs water-coordinated species). Quantitatively, the Dy complex is determined to be evenly partitioned between water and IL-coordinated speciation at 50% (50mM $Dy(OTf)_3$ solution) water molar fraction. At this concentration, a small fraction (11% green) of a third speciation is observed (Figure 3a). Lowering the water fraction to about 28% (upon higher metal loadings in 100mM $Dy(OTf)_3$ solution) decreases the water-coordinated distribution to 32% partition (Figure 3c).

Using the IR determined speciation concentrations, diffusion coefficient of the water-coordinated complex could be evaluated from voltammetric traces. In this analysis, both semi-integral (SI) and semi-derivative (SD) voltammograms were employed to extract the D values. Figures 3b,d display the SI and SD traces of 50 and 100mM $Dy(OTf)_3$ solutions. Using the limiting SI (m*) and peak SD (ep) currents of Red1 wave, the D values were calculated according to Equations S1 and S2 (Supporting Information) for an irreversible process ([50]). Similarly, the D value of IL-coordinated species could be estimated from the dry solution (35ppm) at Red2 wave, where negligible speciation partition is expected. Obtained D values of both speciation are summarized in Table 1. Note that the extracted D values should be considered as upper limits, due to potential contributions from catalytic component in the total faradaic currents. Obtained diffusion coefficient for IL-coordinated (7.6×10^{-12} m^2/s) complex is comparable to reported values in similar ionic liquids media ($\sim 2 \times 10^{-12}$ m^2/s) ([23,51]). While Dy-H_2O value (3.3×10^{-11} m^2/s) was higher than Dy-IL ones. This is consistent with faster mass transport of the water-coordinated complex, due to lower electrostatic repulsions of the complex in the negatively polarized IL interface.

Based on the obtained results, electrochemical and spectroscopic properties of the heterogeneous speciation could be deconvoluted, as summarized in Table 1. On the one hand, the NIR results revealed a distinct electronic configuration of the coordinated

water to the metal center, compared to free or weakly coordinated molecules. In this analysis, spectroscopic features of IL-coordination are not observed (blank) in the studied NIR region. Monitoring the vibrational changes of triflate anions at different water content demonstrated the evolution of the spectrum from one species to a mixture speciation. More specifically, the water coordination led to substantial vibrational downshift of the coordinated triflate anions. As a result of triflate anions displacement by water molecules, the metal complex is partitioned between water-coordinated and IL-coordinated speciation. These observations are in perfect agreement with voltammetric interpretation of the double featured reduction process.

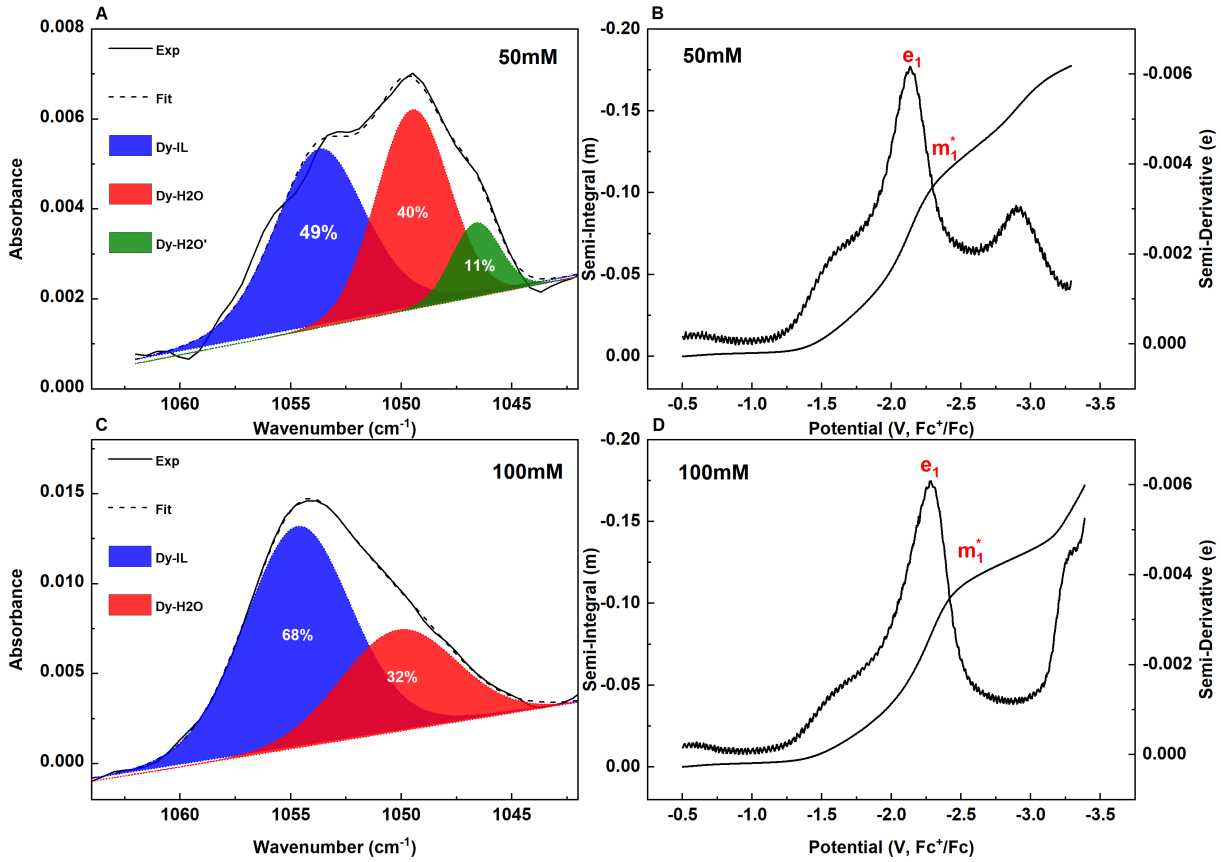

Figure 3. A,C) Deconvoluted IR spectra and B,D) corresponding semi-derivative (SI) and semi-integrals (SD) traces at 50 and 100mM $Dy(OTf)_3$ in BMPyOTf at $[H_2O]$= 500ppm.

In these perspectives, the mechanism for the $Dy(OTf)_3$ reduction in BMPyOTf would be described by three pathways. In highly dry environment, where water molar fraction x_{H2O} (water/$Dy(OTf)_3$ %) is very small (~5%), the Dy is fully (strongly) coordinated to IL-anions and reduced in a consecutive (1+2e-) process. In this process, the very negative (-3.3V) 2e- reduction to Dy metal could be coupled to chemical reaction (EC/EC'), leading to negligible and/or unstable (no stripping peak) metal electrodeposition at the electrode

surface. Introduction of water at low concentrations (5% < x_{H2O} < 30%) leads to displacement of the IL-ligand to the metal center and significant partitioning into water-coordinated complex, resulting in emergence of new reduction wave (Red1) at positive potentials (-2.4V). Within this heterogeneity, the remaining fraction of the IL-coordinated speciation could still be reduced at more negative potentials in a consecutive process. In wet conditions (>30%), the water impact may go beyond metal coordination and ligands displacement, by triggering the catalytic HER. This effect is likely due to increasing the concentration of free or weakly-coordinated water molecules. As a consequence of coupling to the electrodeposition to the fast-catalytic process (HER), both reduction waves (Red1 and Red2) are substantially shifted to more positive potentials (Figure 1d). It is worth noting that the correlation between bulk distribution of the heterogeneous speciation and reduction currents may be restricted to voltammetric timescales. Under extended chronoamperometric conditions, such correlation becomes highly convoluted upon changes in interfacial concentrations. According to Equation 1, the triflate anion concentration at the interface is expected to increase during continuous metal electrodeposition, shifting the equilibrium towards IL-coordinated Dy speciation. As a result, Dy reduction would ultimately be driven under the thermodynamics of Red2 process. This is consistent with previously reported decrease in voltammetric current of Red1, relative to Red2, at multiple potential scans ([37]).

Table 1. Electrochemical and spectroscopic properties of the observed Dy speciation

Dy Speciation	E_{red} (V vs Fc^+/Fc)	D (m^2/s)	NIR (1850 –2000, nm)	IR (cm^{-1})
Dy-IL	-3.3	7.6×10^{-12}	Blank	1334; 1054
Dy-H_2O	-2.4	3.3×10^{-11}	1970	1322; 1050

3) Electrodeposition:

Based on voltammetric analysis, water introduction was shown to shift the reduction process to more positive potentials and lead to substantial increase in current densities. Similar observations were reported in Nd and Eu reduction in water-rich ionic liquid solutions ([33,34]). However, the impact of water addition on the electrodeposition metrics and/or product quality has not been well investigated. In the present work, electrodeposition metrics including the faradaic efficiency (FE) and electrodeposition rates as well as metal stability and purity are examined in water-added solutions.

Metal electrodeposition is highly dictated by the mechanism and dynamics of adatoms formation and adsorption on the electrified electrode surface. Hence, to assess the water impact on the nucleation process, chronoamperometric experiments were carried out at different water contents and constant applied potential. Figure S5 displays the

acquired current densities at applied potential -3V vs Fc^+/Fc and water concentrations ranging from 300 to 3500ppm. Consistent with previously reported profile, the observed traces are typical for the three-dimensional crystal nucleation/growth process followed by diffusion-controlled process ([16,52,53]). It is noteworthy that faster nucleation processes are observed with the increase of water content, as illustrated by higher peak currents (J_m) values (Figure S5). This is also consistent with emergence of stripping peak in the voltammetric scans upon increasing the water content. The nucleation process was examined based on the dimensionless parameters $(J/J_m)^2$ vs (t/t_m), obtained from chronoamperometry results and using the theoretical Scharifker and Hills models (Equations S3 and S4 in the supporting information) for the instantaneous and progressive processes ([54]). From the dimensionless traces, the Dy electrocrystallization appears to follow an instantaneous nucleation process at low water concentration (Figure 4a). Remarkably, increasing the water content seems to switch the nucleation from an instantaneous to a progressive process. This effect indicates that water introduction boosts the rate of crystals growth, as compared to nucleation process. Such observation could also be suggestive of an instantaneous nucleation at the first wave (Red1), while the second wave (Red2) seems to follow a progressive process. These results are consistent with observed changes on the nucleation process with applied overpotentials ([37]).

In evaluating the impact of water content on the electrodeposition metrics, faradaic efficiencies and deposition rates were initially determined at different applied potentials (Figure 4b) in a constant water concentration. In these experiments, the passing charge was maintained at 1C/cm^2 in all studied conditions, preventing possible variations due to deposited amount or film thickness. As expected from the voltammetric response, increasing the overpotentials led to a significant increase in deposition rates. Remarkably, the FE values seem to increase at more negative applied potentials. To further examine the changes in system efficiency, electrodeposition experiments were carried out at different water content. Given the highly negative reduction potential of Red2 in highly dried conditions (35ppm), the deposition was run at an applied potential about -3.3V. Note that even at these very negative potentials, the deposition current was still small (< 0.2 mA/cm^2). In these dried conditions, negligible deposit amount could be obtained when passing over 1C/cm^2, leading to very low FE values (<2%). Consistent with the emergence of the positive voltammetric wave (Red1) at positive potentials (-2.4V), water addition boosted the deposition rate by about one order. Moreover, the FE values increased by almost two orders of magnitude when transitioning from the dried (35ppm) to wet (3500ppm) environment. Such FE increase could be correlated to rate improvement in crystal growth, under progressive nucleation process. Examination of chronoamperometric traces as a function of time exhibited a severe decay, when small positive potentials (-2.3V) were applied (Figure S8). Given the

3e- nature reduction of Red1, metal electrodeposition wave leads to co-release of triflate anions (Equation 1). As a result of such interfacial increase of anion concentration, the speciation equilibrium is predicted to shift towards IL-coordinated complex, requiring larger reduction overpotentials. Thus, more sustainable currents could only be obtained upon electrodeposition at Red2 potentials. These interfacial equilibria would eventually affect the robustness of system efficiency. In fact, monitoring the faradaic efficiency as a function of passing charge, reveals a substantial decay in FE values by about 30%, at higher deposition scales (Figure S6). Due to concentration buildup of triflate anions at the interface, passing higher charges would essentially promote the IL-coordinated speciation, shifting the reduction to dominantly Red2 process. As indicated by voltammetric analysis, Red2 appears to be more coupled with HER reaction, which would decrease the overall faradaic efficiency. Chromatographic (GC) analysis of the headspace during and post electrodeposition experiments performed at Red2 potentials, reveals considerable release of hydrogen gas evolution (Figure S7). Hence, the change in interfacial concentrations and speciation are likely the main factors of severe decays in both chronoamperometric currents at Red1 potentials as well as faradaic efficiency under extended electrodeposition timescales.

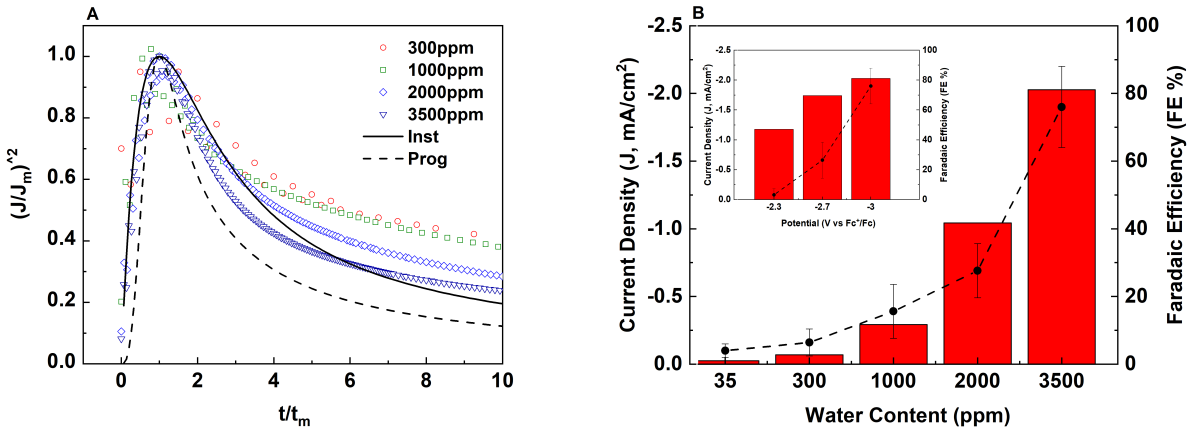

Figure 4. A) Dimensionless chronoamperometric traces recorded at different water contents (ppm) and theoretical traces for instantaneous and progressive nucleation processes. B) FE(%) and chronoamperometric current densities of 100mM $Dy(OTf)_3$ in BMPyOTf at different water contents (ppm). Inset: FE% and J values at different applied potentials at $[H_2O]$= 3500ppm.

To examine the nature and composition of the obtained electrodeposited materials in the presence of water, surface and elemental analyses were performed. Characterization of Dy oxidation state in the electrodeposited material was carried out using XPS analysis. As demonstrated above and regardless of water content, the electrodeposition would ultimately proceed via the thermodynamics of Red2 wave, due to dominant interfacial concentration of Dy-IL speciation. On this basis, the XPS analysis was carried out for obtained electrodeposit in water-rich environment, enabling to assess the metal stability under wet conditions. Previously, we reported the XPS spectrum of the electrodeposited materials, which exhibited a centered peak at 1296eV ([37]). This feature was assigned to

zero valent metal, based on similarities with reported experimental and theoretical characteristics binding energies, 1296 and 1289eV for Dy metal and oxide, respectively ([23,55]). In the present analysis, further XPS analysis was performed, including surface sputtering and acquisition of Dy oxide (Dy_2O_3) as a standard sample (Figure **5**a,b).

Examination of the high resolution Dy3d spectra shows no clear differences in binding energies upon surface sputtering, as both spectra exhibited peaks at about 1295eV ±1eV (Figure 5a). In addition, the spectra were quite comparable to recorded spectrum for Dy_2O_3 oxide, without evidence of theoretically predicted 7eV difference in binding energies, between Dy metal (1296eV) and oxide (1289eV) ([55]). In contrast to these theoretical predictions, Barreca et al. reported 1296.5eV as an experimental characteristic for the Dy_2O_3 oxide substrate ([56]). Given such ambiguity between theoretical and experimental characteristics of Dy3d signals, Dy4d spectra of these samples were then recorded and obtained results are displayed in Figure 5b. While interpretation of convoluted Dy4d spectrum could be more complex than Dy3d, the multi features, sharpness and distinct peak separation may be more informative regarding the presence of zero valent Dy metal ([55]). In this analysis, the unsputtered deposit exhibited similar features to Dy_2O_3 standard, with broad band at 156eV and a shouldering peak at 153eV ([28,51]). Remarkably, surface sputtering of the deposit improved the peaks sharpness, as well as significant separation between 153 and 156eV

peaks. In addition to these variations, two new peaks appear to emerge at 158 and 161eV. On the one hand, the splitting peaks at 156 and 158 eV, due to 4d core pin-orbit interactions, have been reported as characteristics for DyF_3 ([57]). This is consistent with the substantial increase (from 8.6 to 22.9 atomic%) that can be seen in the F signal upon sputtering (Figure S9 and Table S2). On the other hand, the increased sharpness and separation of the peak at 153eV, as well as the emerging broad (due to overlap with S2p at 162eV) peak at 161eV could be indicative of Dy metal presence ([55]). As illustrated by the fitting traces in Figure 5b (dashed traces), the surface sputtering reveals clear formation of DyF_3 and possible presence of Dy metal in the bulk of the deposited material. In conjunction with reported experimental binding energies, the overall XPS results are mostly suggestive for the presence of mixture of Dy_2O_3, DyF_3 and Dy metal form in the electrodeposited product. Given the high caution in handling the electrodeposited material under inert atmosphere, the Dy metal oxidation and fluorination are more likely due to chemical reactivity of the reduced Dy metal (EC mechanism) with the water and electrolyte components. This is consistent with HER evolution during electrodeposition experiments and the drop in system efficiency at extended timescales.

Given the observed impact of water addition on the nucleation process, morphology analysis of obtained deposits at different water contents was carried out using SEM

technique. As displayed in Figure 5c,d, the electrodeposited films had generally a powdery form with dendritic particles of sub micrometers diameters. While the same charge density (1C/cm^2) was passed for the obtained deposits, changing the water content had significant impact on the particle morphology. At higher water content, the particles become denser and more aggregated, with heterogeneous surfaces between rough and smooth regions (Figure 5d). These morphologic differences are consistent with observed changes in the nucleation process from spontaneous and progressive regimes with increase of water content. This is also well correlated with observed deposition rates between low and high-water content, under chronoamperometric conditions.

Irrespective of Dy oxidation state and morphologic structure, quantification of Dy content in the electrodeposited material, obtained in two different water contents, was performed. In this analysis, Dy surface composition was determined using EDS characterization. Reported REE compositions in obtained electrodeposits from ionic liquids are range from 10 to 75% ([4,16,27,40,58,59]), mostly based on surface analysis by EDS. Elemental compositions from EDS analysis in the electrodeposited films are displayed in Figure 5c,d. Surface composition of both samples included significant contents of O, F, C and S elements, which likely originate from the electrolyte components. In agreement with faradaic efficiencies, very small (~5%) Dy content is observed in obtained films

deposited in the low water conditions, while it increased by 1 order of magnitude in the prepared deposit obtained in water-rich media.

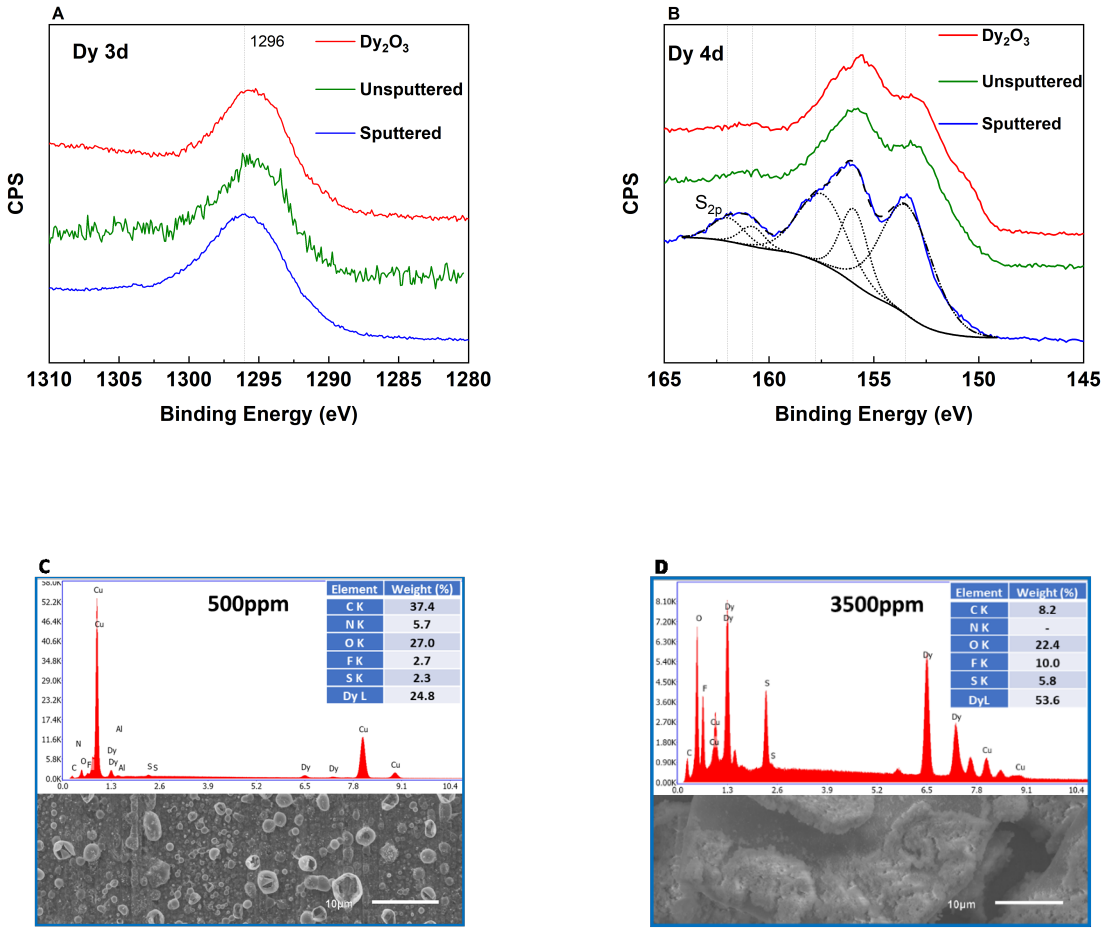

Figure 5. Recorded XPS spectra in A) Dy3d and B) Dy4d regions of the Dy_2O_3 standard and obtained electrodeposited film Dy in BMPyOTf on Cu electrode, at $[H_2O]$=3500ppm. SEM images of obtained electrodeposited Dy in BMPyOTf on Cu electrode, at C) 500ppm and D) 3500ppm water contents. Insets: corresponding EDX spectra and

elemental compositions.

In a separate characterization with TXRF technique, Dy content was alternatively evaluated based on the weighted mass of electrodeposited materials obtained in water-rich conditions (Table S1). The results indicated that bulk-based (deposit mass) Dy composition compares well with surface-based values, suggesting a homogeneous embedment of the Dy and electrolyte elements in the bulk deposit. With an average about 60%, obtained Dy purity in wet conditions is comparable to reported values in ionic liquids electrolytes. Considering the observed severe decays in both FE values and voltammetric stripping ratios under long electrodeposition timescales (high passing charge), only a very small fraction (probably <15%) of the total (60%) Dy content is expected to stabilize as Dy zero valent metal. Yet, a conclusive determination of the Dy zero valent metal under these limited purity levels may not be straight forward from surface (XPS) analysis. Further post-processing of the electrodeposited materials might be required in order to determine the actual content of the Dy zero valent metal in these deposits.

CONCLUSION: In this work, interplays of the impact of water introduction on the Dy electrodeposition in pyrrolidinium triflate system were investigated. Interpretation of the electrodeposition process is discussed as a function of solvation and coordination interactions and the evolving speciation heterogeneity. The results of the mechanistic

analysis were correlated to the observed electrodeposition metrics and product properties. The overall impact of water introduction seems to engender both promoting and mitigating effects on the Dy electrodeposition process.

In dry conditions, the reduction proceeds via consecutive (1+2e-) mechanism, where solvation of the Dy complex is predominantly characterized by full IL-coordination. As a result of full IL-coordination, Dy reduction to its zero valent metal occurs at very negative potentials (Red2). However, the electrodeposition under these conditions seems to be unstable and inefficient. Initial introduction of water traces appears to overcome these limitations, leading to a partial partitioning of Dy complex into highly water-coordinated speciation. This resulted in the emergence of a new 3e- wave at more positive potentials (Red1). In addition to displacement of IL-coordination, water introduction led to a faster electrocrystallization process. In this perspective, presence of water could be essential to sustain the structured ionic liquid interface through neutralizing the electrostatic interactions between IL components and released triflate anions upon metal reduction. Higher water addition results in the solvation of the remaining Dy fraction, leading to significant shift of Red2 process. This shift is shown to be correlated with the coupling of Red2 process with HER under wet conditions. Parallel to these coordination effects on speciation and reduction mechanism, water presence is demonstrated to alter the chemical stability of the zero valent Dy metal under long

electrodeposition conditions. This aspect was predicted from stripping voltammetry and consolidated by XPS analysis. Furthermore, evaluation of the Dy content at the surface and bulk of the obtained electrodeposited material shows a limited purity (~60%), with substantial contamination by electrolyte components. These results were also consistent with severe decay in system efficiency, under extended deposition scale.

In summary, the present work reveals a complex interplay of water effects on the electrodeposition process of Dy in the studied ionic liquid. On the one hand, water seems to have promoting effects via coordination interactions and structural sustainability of the IL interface, lowering the thermodynamics of the reduction and boosting the crystal growth and deposition rate. On the other hand, presence of water represents an immediate oxidative environment that mitigates the chemical stability of the zero valent Dy metal and robustness of the system efficiency. Under voltammetric timescale, the hydrophobic ionic liquid interface could provide a protective environment for the reduced materials. Under long electrolytic conditions, water may still destroy the ionic liquid layer and oxidize the reduced material. As a result of direct or indirect water electrolysis, HER becomes prominent and leads to severe decay of faradaic efficiency. In these perspectives, the promoting effects of water introduction on REE electrodeposition in ionic liquid must be envisioned within the overall system performance. Electrodeposition metrics such as rate (kinetics) and energy efficiency

(thermodynamics) may indeed be improved by additives (water) introduction. Nevertheless, high metal stability and purity ultimately remain the major components for the competitiveness of the IL technology. Though, techno-economic assessment (TEA) shall be more informing about the viability of the overall process, at a given cost, production rate and metal content. After more than a decade of research efforts, the development of the IL process has faced major challenges, with most remaining at the chemistry level. Therefore, more innovative strategies are still sought to promote the IL technology as an alternative for the industrial molten salt process.

ASSOCIATED CONTENT

Supporting Information. The Supporting Information is available free of charge online.

Electrochemical equations; additional figures; cyclic voltammetry; chronoamperometry; FTIR; faradaic efficiency; TXRF; XPS; GC; additional tables (Word Document)

AUTHOR INFORMATION

Corresponding Author

* A. Atifi. *abderrahman.atifi@inl.gov*

Author Contributions

The manuscript was written through contributions of all authors. All authors have given approval to the final version of the manuscript.

Funding Sources

This work was funded by the US Department of Energy through the Critical Materials Institute and performed at INL under DOE Idaho Operations Office Contract DE AC07 05ID14517. This work was partially performed through the DOE Science Undergraduate Laboratory Internships (SULI) program for K.O.

ACKNOWLEDGMENT

The authors would like to express their gratitude to Paulo Perez (University of Utah) for his help in XPS experiments. The authors gratefully acknowledge the assistance of Megha Dubey in running SEM-EDS experiments at the Microscopy and Characterization Suite (MaCS) facility of the Center for Advanced Energy Studies (CAES) at INL.

REFERENCES

(1) Binnemans, K.; Jones, P. T.; Blanpain, B.; Van Gerven, T.; Yang, Y.; Walton, A.; Buchert, M. Recycling of Rare Earths: A Critical Review. *J. Clean. Prod.* **2013**, *51*,

1–22. https://doi.org/10.1016/j.jclepro.2012.12.037.

(2) Weng, Z.; Haque, N.; Mudd, G. M.; Jowitt, S. M. Assessing the Energy Requirements and Global Warming Potential of the Production of Rare Earth Elements. *J. Clean. Prod.* **2016**, *139*, 1282–1297. https://doi.org/10.1016/j.jclepro.2016.08.132.

(3) Yang, Y.; Walton, A.; Sheridan, R.; Güth, K.; Gauß, R.; Gutfleisch, O.; Buchert, M.; Steenari, B. M.; Van Gerven, T.; Jones, P. T.; Binnemans, K. REE Recovery from End-of-Life NdFeB Permanent Magnet Scrap: A Critical Review. *J. Sustain. Metall.* **2017**, *3* (1), 122–149. https://doi.org/10.1007/s40831-016-0090-4.

(4) Binnemans, K.; Jones, P. T.; Müller, T.; Yurramendi, L. Rare Earths and the Balance Problem: How to Deal with Changing Markets? *J. Sustain. Metall.* **2018**, *4* (1), 126–146. https://doi.org/10.1007/s40831-018-0162-8.

(5) Han, W.; Li, M.; Zhang, M. L.; Yan, Y. De. Progress in Preparation of Rare Earth Metals and Alloys by Electrodeposition in Molten Salts. *Rare Metals*. 2016, pp 811–825. https://doi.org/10.1007/s12598-016-0798-0.

(6) Vahidi, E.; Zhao, F. Assessing the Environmental Footprint of the Production of Rare Earth Metals and Alloys via Molten Salt Electrolysis. *Resour. Conserv. Recycl.* **2018**, *139* (August), 178–187. https://doi.org/10.1016/j.resconrec.2018.08.010.

(7) Glukhov, L. M.; Greish, A. A.; Kustov, L. M. Electrodeposition of Rare Earth

Metals Y, Gd, Yb in Ionic Liquids. *Russ. J. Phys. Chem. A* **2010**, *84* (1), 104–108. https://doi.org/10.1134/S0036024410010206.

(8) Binnemans, K. Lanthanides and Actinides in Ionic Liquids. *Chemical Reviews*. 2007, pp 2592–2614. https://doi.org/10.1021/cr050979c.

(9) Liu, F.; Deng, Y.; Han, X.; Hu, W.; Zhong, C. Electrodeposition of Metals and Alloys from Ionic Liquids. *J. Alloys Compd.* **2016**, *654*, 163–170. https://doi.org/10.1016/j.jallcom.2015.09.137.

(10) Adams, D. J.; Dyson, P. J.; Tavener, S. J. *Chemistry in Alternative Reaction Media*; Wiley, 2003. https://doi.org/10.1002/0470869666.

(11) Kerton, F.; Marriott, R. *Alternative Solvents for Green Chemistry*, 2nd ed.; Green Chemistry Series; Royal Society of Chemistry: Cambridge, 2013. https://doi.org/10.1039/9781849736824.

(12) Silvester, D. S.; Compton, R. G. Electrochemistry in Room Temperature Ionic Liquids: A Review and Some Possible Applications. *Zeitschrift für Phys. Chemie* **2006**, *220* (10), 1247–1274. https://doi.org/10.1524/zpch.2006.220.10.1247.

(13) Tsuda, T.; Hussey, C. L. *Electrochemistry of Room-Temperature Ionic Liquids and Melts*; 2009. https://doi.org/10.1007/978-1-4419-0655-7_2.

(14) Fedorov, M. V; Kornyshev, A. A. Ionic Liquids at Electrified Interfaces. *Chemical Reviews*. 2014, pp 2978–3036. https://doi.org/10.1021/cr400374x.

(15) Kondo, H.; Matsumiya, M.; Tsunashima, K.; Kodama, S. Attempts to the Electrodeposition of Nd from Ionic Liquids at Elevated Temperatures. *Electrochim. Acta* **2012**, *66*, 313–319. https://doi.org/10.1016/j.electacta.2012.01.101.

(16) Kazama, R.; Matsumiya, M.; Tsuda, N.; Tsunashima, K. Electrochemical Analysis of Diffusion Behavior and Nucleation Mechanism for Dy(II) and Dy(III) in Phosphonium-Based Ionic Liquids. *Electrochim. Acta* **2013**, *113*, 269–279. https://doi.org/10.1016/j.electacta.2013.09.082.

(17) Ishii, M.; Matsumiya, M.; Kawakami, S. Development of Recycling Process for Rare Earth Magnets by Electrodeposition Using Ionic Liquids Media. *ECS Trans.* **2013**, *50* (11), 549–560. https://doi.org/10.1149/05011.0549ecst.

(18) Kondo, H.; Matsumiya, M.; Tsunashima, K.; Kodama, S. Investigation of Oxidation State of the Electrodeposited Neodymium Metal Related with the Water Content of Phosphonium Ionic Liquids. *ECS Trans.* **2013**, *50* (11), 529–538. https://doi.org/10.1149/05011.0529ecst.

(19) Ota, H.; Matsumiya, M.; Sasaya, N.; Nishihata, K.; Tsunashima, K. Investigation of Electrodeposition Behavior for Nd(III) in [P2225][TFSA] Ionic Liquid by EQCM Methods with Elevated Temperatures. *Electrochim. Acta* **2016**, *222*, 20–26. https://doi.org/10.1016/j.electacta.2016.11.038.

(20) Ishioka, K.; Matsumiya, M.; Ishii, M.; Kawakami, S. Development of Energy-Saving Recycling Process for Rare Earth Metals from Voice Coil Motor by Wet

Separation and Electrodeposition Using Metallic-TFSA Melts. *Hydrometallurgy* **2014**, *144–145*, 186–194. https://doi.org/10.1016/j.hydromet.2014.02.007.

(21) Matsumiya, M.; Yamada, T.; Kikuchi, Y.; Kawakami, S. Removal of Iron and Boron by Solvent Extraction with Ionic Liquids and Recovery of Neodymium Metal by Direct Electrodeposition. *Solvent Extr. Ion Exch.* **2016**, *34* (6), 522–534. https://doi.org/10.1080/07366299.2016.1218692.

(22) Lodermeyer, J.; Multerer, M.; Zistler, M.; Jordan, S.; Gores, H. J.; Kipferl, W.; Diaconu, E.; Sperl, M.; Bayreuther, G. Electroplating of Dysprosium, Electrochemical Investigations, and Study of Magnetic Properties. *J. Electrochem. Soc.* **2006**, *153* (4), C242. https://doi.org/10.1149/1.2172548.

(23) Kurachi, A.; Matsumiya, M.; Tsunashima, K.; Kodama, S. Electrochemical Behavior and Electrodeposition of Dysprosium in Ionic Liquids Based on Phosphonium Cations. *J. Appl. Electrochem.* **2012**, *42* (11), 961–968. https://doi.org/10.1007/s10800-012-0463-8.

(24) Matsumiya, M.; Kikuchi, Y.; Yamada, T.; Kawakami, S. Extraction of Rare Earth Ions by Tri-n-Butylphosphate/Phosphonium Ionic Liquids and the Feasibility of Recovery by Direct Electrodeposition. *Sep. Purif. Technol.* **2014**, *130*, 91–101. https://doi.org/10.1016/j.seppur.2014.04.021.

(25) Matsumiya, M.; Kazama, R.; Tsunashima, K. Analysis of Coordination States for Dy(II) and Dy(III) Complexes in Ionic Liquids by Raman Spectroscopy and DFT

Calculation. *J. Mol. Liq.* **2016**, *215*, 308–315. https://doi.org/10.1016/j.molliq.2015.12.049.

(26) Kuribara, K.; Matsumiya, M.; Tsunashima, K. Solvation Structure and Thermodynamics for Pr(III), Nd(III) and Dy(III) Complexes in Ionic Liquids Evaluated by Raman Spectroscopy and DFT Calculation. *J. Mol. Struct.* **2016**, *1125*, 186–192. https://doi.org/10.1016/j.molstruc.2016.06.059.

(27) Bourbos, E.; Giannopoulou, I.; Karantonis, A.; Paspaliaris, I.; Panias, D. Reduction of Light Rare Earths and a Proposed Process for Nd Electrorecovery Based on Ionic Liquids. *J. Sustain. Metall.* **2018**, *4* (3), 395–406. https://doi.org/10.1007/s40831-018-0186-0.

(28) Suppan, G.; Ruehrig, M.; Kanitz, A.; Gores, H. J. Electroplating Dysprosium from IL-Based Solutions: A Promising Electrochemical Step to Produce Stronger High Performance Nd(Dy)-Fe-B Sintered Magnets. *J. Electrochem. Soc.* **2015**, *162* (8), D382–D388. https://doi.org/10.1149/2.0911508jes.

(29) Oono, N.; Sagawa, M.; Kasada, R.; Matsui, H.; Kimura, A. Production of Thick High-Performance Sintered Neodymium Magnets by Grain Boundary Diffusion Treatment with Dysprosium-Nickel-Aluminum Alloy. *J. Magn. Magn. Mater.* **2011**, *323* (3–4), 297–300. https://doi.org/10.1016/j.jmmm.2010.09.021.

(30) Bagri, P.; Luo, H.; Popovs, I.; Thapaliya, B. P.; Dehaudt, J.; Dai, S. Trimethyl Phosphate Based Neutral Ligand Room Temperature Ionic Liquids for

Electrodeposition of Rare Earth Elements. *Electrochem. commun.* **2018**, *96* (September), 88–92. https://doi.org/10.1016/j.elecom.2018.10.001.

(31) Krishna, G. M.; Rout, A.; Venkatesan, K. A. Voltammetric Investigation of Some Lanthanides in Neutral Ligand-Ionic Liquid. *J. Electroanal. Chem.* **2020**, *856*, 113671. https://doi.org/10.1016/j.jelechem.2019.113671.

(32) Geysens, P.; Lin, P. C.; Fransaer, J.; Binnemans, K. Electrodeposition of Neodymium and Dysprosium from Organic Electrolytes. *Phys. Chem. Chem. Phys.* **2021**, *23* (15), 9070–9079. https://doi.org/10.1039/d0cp06606k.

(33) Sanchez-Cupido, L.; Pringle, J. M.; Siriwardana, A. L.; Unzurrunzaga, A.; Hilder, M.; Forsyth, M.; Pozo-Gonzalo, C. Water-Facilitated Electrodeposition of Neodymium in a Phosphonium-Based Ionic Liquid. *J. Phys. Chem. Lett.* **2019**, *10* (2), 289–294. https://doi.org/10.1021/acs.jpclett.8b03203.

(34) Ehrenburg, M. R.; Molodkina, E. B.; Mishchenko, A.; Rudnev, A. V. The Promoting Effect of Water on the Electrodeposition of Eu in a Dicyanamide Ionic Liquid. *Electrochim. Acta* **2021**, *379*. https://doi.org/10.1016/j.electacta.2021.138169.

(35) Small, L. J.; Sears, J. M.; Lambert, T. N.; Boyle, T. J.; Hess, R. F. Electroreduction of Er3+ in Nonaqueous Solvents. *RSC Adv.* **2016**, *6* (92), 89564–89571. https://doi.org/10.1039/c6ra15061f.

(36) Sanchez-Cupido, L.; Pringle, J. M.; Siriwardana, A. I.; Hilder, M.; Forsyth, M.;

Pozo-Gonzalo, C. Correlating Electrochemical Behavior and Speciation in Neodymium Ionic Liquid Electrolyte Mixtures in the Presence of Water. *ACS Sustain. Chem. Eng.* **2020**, *8* (37), 14047–14057. https://doi.org/10.1021/acssuschemeng.0c04288.

(37) Atifi, A.; Baek, D. L.; Fox, R. V. Electrodeposition of Dysprosium in Pyrrolidinium Triflate Ionic Liquid at Ambient Temperature: Unraveling System Efficiency and Impact of Solvation Interplays on the Reduction Process. *Electrochim. Acta* **2021**, *378*, 138140. https://doi.org/10.1016/j.electacta.2021.138140.

(38) Bengio, D.; Dumas, T.; Arpigny, S.; Husar, R.; Mendes, E.; Solari, P. L.; Schlegel, M. L.; Schlegel, D.; Pellet-Rostaing, S.; Moisy, P. Electrochemical and Spectroscopic Study of EuIII and EuII Coordination in the 1-Ethyl-3-Methylimidazolium Bis(Trifluoromethylsulfonyl)Imide Ionic Liquid. *Chem. - A Eur. J.* **2020**, 14385–14396. https://doi.org/10.1002/chem.202001469.

(39) Zhao, C.; Bond, A. M.; Lu, X. Determination of Water in Room Temperature Ionic Liquids by Cathodic Stripping Voltammetry at a Gold Electrode. *Anal. Chem.* **2012**, *84* (6), 2784–2791. https://doi.org/10.1021/ac2031173.

(40) Sanchez-Cupido, L.; Pringle, J. M.; Siriwardana, A.; Pozo-Gonzalo, C.; Forsyth, M. Electrochemistry of Neodymium in Phosphonium Ionic Liquids: The Influence of Cation, Water Content, and Mixed Anions. *Aust. J. Chem.* **2020**, *73*

(11), 1080–1087. https://doi.org/10.1071/CH19581.

(41) Atifi, A.; Ryan, M. D. Electrochemistry and Spectroelectrochemistry of 1,4-Dinitrobenzene in Acetonitrile and Room-Temperature Ionic Liquids: Ion-Pairing Effects in Mixed Solvents. *Anal. Chem.* **2014**, *86* (13), 6617–6625. https://doi.org/10.1021/ac5012987.

(42) Atifi, A.; Ryan, M. D. Influence of RTIL Nanodomains on the Voltammetry and Spectroelectrochemistry Of Fullerene C60 in Benzonitrile/Room Temperature Ionic Liquids Mixtures. *Electrochim. Acta* **2016**, *191*, 567–576. https://doi.org/10.1016/j.electacta.2016.01.104.

(43) Atifi, A.; Mak, P. J.; Ryan, M. D. Proton-Coupled Reduction of an Iron Nitrosyl Porphyrin in the Protic Ionic Liquid Nanodomain. *Electrochim. Acta* **2019**, *295*, 735–741. https://doi.org/10.1016/j.electacta.2018.10.179.

(44) Atifi, A.; Boyce, D. W.; DiMeglio, J. L.; Rosenthal, J. Directing the Outcome of CO 2 Reduction at Bismuth Cathodes Using Varied Ionic Liquid Promoters. *ACS Catal.* **2018**, 2857–2863. https://doi.org/10.1021/acscatal.7b03433.

(45) Atifi, A.; Keane, T. P.; Dimeglio, J. L.; Pupillo, R. C.; Mullins, D. R.; Lutterman, D. A.; Rosenthal, J. Insights into the Composition and Function of a Bismuth-Based Catalyst for Reduction of CO2 to CO. *J. Phys. Chem. C* **2019**, *123* (14), 9087–9095. https://doi.org/10.1021/acs.jpcc.9b00504.

(46) Atifi, A.; Ryan, M. D. Spectroscopic Evidence of Nanodomains in THF/RTIL

Mixtures: Spectroelectrochemical and Voltammetric Study of Nickel Porphyrins. *Anal. Chem.* **2015**, *87* (24), 12245–12253. https://doi.org/10.1021/acs.analchem.5b03411.

(47) Atifi, A.; Ryan, M. D. Altering the Coordination of Iron Porphyrins by Ionic Liquid Nanodomains in Mixed Solvent Systems. *Chem. - A Eur. J.* **2017**. https://doi.org/10.1002/chem.201701540.

(48) Rahman, M. H.; Atifi, A.; Rosenthal, J.; Ryan, M. D. Reversible Proton-Coupled Reduction of an Iron Nitrosyl Porphyrin within [DBU-H]+-Based Protic Ionic Liquid Nanodomains. *Inorg. Chem.* **2021**, *60* (14), 10631–10641. https://doi.org/10.1021/acs.inorgchem.1c01273.

(49) Johnston, D. H.; Shriver, D. F. Vibrational Study of the Trifluoromethanesulfonate Anion: Unambiguous Assignment of the Asymmetric Stretching Modes. *Inorg. Chem.* **1993**, *32* (6), 1045–1047. https://doi.org/10.1021/ic00058a050.

(50) Goto, M.; Oldham, K. B. Semiintegral Electroanalysis: Shapes of Neopolarograms. *Anal. Chem.* **1973**, *45* (12), 2043–2050. https://doi.org/10.1021/ac60334a027.

(51) Berger, C. A.; Arkhipova, M.; Maas, G.; Jacob, T. Dysprosium Electrodeposition from a Hexaalkylguanidinium-Based Ionic Liquid. *Nanoscale* **2016**, *8* (29), 13997–14003. https://doi.org/10.1039/c6nr01351a.

(52) Zhou, X.; Wang, Y.; Liang, Z.; Jin, H. Electrochemical Deposition and Nucleation/Growth Mechanism of Ni-Co-Y2O3 Multiple Coatings. *Materials (Basel)*. **2018**, *11* (7). https://doi.org/10.3390/ma11071124.

(53) Hyde, M. E.; Compton, R. G. A Review of the Analysis of Multiple Nucleation with Diffusion Controlled Growth. *J. Electroanal. Chem.* **2003**, *549* (SUPPL.), 1–12. https://doi.org/10.1016/S0022-0728(03)00250-X.

(54) Scharifker, B.; Hills, G. Theoretical and Experimental Studies of Multiple Nucleation. *Electrochim. Acta* **1983**, *28* (7), 879–889. https://doi.org/10.1016/0013-4686(83)85163-9.

(55) Moulder, J. F. *Handbook of X-Ray Photoelectron Spectroscopy: A Reference Book of Standard Spectra for Identification and Interpretation of XPS Datale*, illustrate.; Chastain, J., Ed.; Physical Electronics Division, Perkin-Elmer Corporation, 1992.

(56) Barreca, D.; Gasparotto, A.; Milanov, A.; Tondello, E.; Devi, A.; Fischer, R. A. Nanostructured Dy 2 O 3 Films: An XPS Investigation . *Surf. Sci. Spectra* **2007**, *14* (1), 52–59. https://doi.org/10.1116/11.20080702.

(57) Li, Y.; Li, T.; Zhu, X.; Alshehri, A. A.; Alzahrani, K. A.; Lu, S.; Sun, X. DyF3: An Efficient Electrocatalyst for N2 Fixation to NH3 under Ambient Conditions. *Chem. - An Asian J.* **2020**, *15* (4), 487–489. https://doi.org/10.1002/asia.201901624.

(58) Matsumiya, M.; Ishii, M.; Kazama, R.; Kawakami, S. Electrochemical Analyses

of Diffusion Behaviors and Nucleation Mechanisms for Neodymium Complexes in [DEME][TFSA] Ionic Liquid. *Electrochim. Acta* **2014**, *146*, 371–377. https://doi.org/10.1016/j.electacta.2014.09.066.

(59) Ota, H.; Matsumiya, M.; Yamada, T.; Fujita, T.; Kawakami, S. Purification of Rare Earth Bis(Trifluoromethyl-Sulfonyl)Amide Salts by Hydrometallurgy and Electrodeposition of Neodymium Metal Using Potassium Bis(Trifluoromethyl-Sulfonyl)Amide Melts. *Sep. Purif. Technol.* **2016**, *170*, 417–426. https://doi.org/10.1016/j.seppur.2016.06.044.

Synopsis TOC

The overall viability of water additives for the electrochemical production of rare earth metals in ionic liquids was investigated.